Day-to-day variability of VTEC and ROTI in October 2012 with impact of high-speed solar wind stream on 13 October 2012

Ilyasse Azzouzi, Y. Migoya-Orué, P Coïsson, Christine Amory-Mazaudier, Rolland Fleury, S.M. Radicella

Day-to-day variability of VTEC and ROTI in October 2012 with impact of high-speed solar wind stream on 13 October 2012

Azzouzi, I.[1, 2], Migoya-Orue, Y. O.[3], Coïsson, P.[4], Amory Mazaudier, C.[1,3], Fleury, R.[5], Radicella, S.M.[3]

[1] LPP/UPMC/Polytechnique/CNRS, University Pierre and Marie Curie Paris France.
[2] LA2I / EMI / University Mohammed V Agdal Rabat, Morocco.
[3] T/ICT4D, Abdus Salam International Centre for Theoretical Physics, Trieste, Italy
[4] Institut de Physique du Globe de Paris, Sorbonne Paris Cité, Univ Paris Diderot, CNRS, Paris, France.
[5] MO - Dépt. Micro-Ondes/Lab-STICC /UMR CNRS 6285 - Télécom Bretagne – Technopole de Brest-Iroise, France.

E mail (christine.amory@lpp.polytechnique.fr).

Accepted: 7 March 2016

Abstract This paper presents the day-to-day variability of the Vertical Total Electron Content (VTEC) and the Rate of change of TEC Index (ROTI) in October 2012. We focused our attention to the impact of a high-speed solar wind stream (HSSWS) on the ionosphere in middle and low latitudes on 13 October 2012. This event was preceded by two other disturbances caused by a Coronal Mass Ejection (CME) at 05:26UT on 8 October and a HSSWS around 19:00UT on 9 October. The changes in the VTEC observed during the period between 8 and 12 October preceding the 13 October case showed a comparable response of the ionosphere in both hemispheres, varying mainly with latitude and presenting a stronger impact in the Northern hemisphere. The VTEC increased at the arrival of the CME on 8 October, then decreased, and increased again on 13 October. The solar wind speed associated with the second HSSWS reached its peak, 580 km/s around 17:00UT during the recovery phase of a geomagnetic storm started around 00:00UT on 13 October. Its impact was observed in Africa and in Eastern South America on the ROTI, an indicator of ionospheric scintillation. On 13 October, the ROTI was small over whole Africa and in Eastern South America at the moment the impact of the second HSSWS. These observations are interpreted as due to the ionospheric disturbance dynamo electric field associated with the Joule heating produced in the auroral zone by the HSSWS.

Keywords:

1. Introduction

The behavior of the equatorial ionosphere is characterized by four main phenomena: 1) the equatorial fountain and the Equatorial Ionization Anomaly (EIA) (Namba and Maeda, 1939; Appleton, 1946), 2) the Equatorial Electrojet (EEJ) (Chapman 1951), 3) the Pre Reversal Enhancement (PRE) of the zonal electric field (Woodman, 1970), and 4) the Equatorial Plasma Bubbles (EPBs) (Basu and Basu, 1981).

At the geomagnetic equator, the magnetic field is horizontal and the ExB drift, related to the Laplace (Lorentz) force, is vertical. During the daytime, when the zonal electric field is eastward, the plasma moves up, and reaches higher altitudes, where the pressure gradient and gravity forces become significant comparing to the Laplace (Lorentz) force. In these higher altitudes, the plasma is driven by the ambipolar diffusion along the magnetic field lines. This phenomenon is named the equatorial fountain. This fountain effect creates the EIA composed by a trough of density at the equator and two peaks of density in the geomagnetic latitudes 15°N and 15°S.

The EEJ is an electric current flowing in the E-region of the ionosphere (~110km), along the magnetic equator, between 3°N and 3°S geomagnetic latitude. The PRE was observed first at Jicamarca (Woodman, 1970). The equatorial electric field created by the ionospheric dynamo (Stewart, 1882; Chapman and Bartels, 1940) is eastward during the daytime and westward at nighttime. At the time of its reversal, post sunset, the eastward electric field strongly increases, this is called the PRE. The vertical drift (ExB drift) moves up or down the plasma. An eastward/westward electric field lifts up/down the plasma.

The existence of equatorial plasma irregularities, the EPB is attributed to the Generalized Rayleigh-Taylor (R-T) plasma instability (e.g. Kelley, 2009 and references therein). In equatorial latitudes, the R-T plasma instability is triggered by the PRE. At the time of the PRE, the eastward electric field quickly moves up the ionospheric layers and creates large gradients of electron density which is condition for the development of the R-T instability. These irregularities affect the propagation of electromagnetic waves and cause scintillations on the signal of the Global Positioning System (GPS) (Basu and Basu, 1981), spread F on the ionosonde signal (Abdu et al., 1983), or plumes on the incoherent scatter radar signal (Woodman and La Hoz, 1976). It is important to know the variability of these plasma irregularities for operation of the Global Navigation Satellite System (GNSS).

These irregularities also depend on the electrodynamics coupling of ionosphere between in the equatorial and auroral latitudes. This coupling is very strong during geomagnetic disturbances. The auroral currents affect the ionospheric electric fields and currents, and the thermospheric circulation of a global scale. Two main physical processes are well known: the prompt penetration of the magnetospheric convection electric field (Vasyliunas, 1970) and the ionospheric disturbance dynamo (Blanc and Richmond, 1980). The electric field disturbance related to the prompt penetration is named the Prompt Penetration Electric Field (PPEF), and the electric field due to the ionospheric disturbance dynamo is named the Disturbance Dynamo Electric Field (DDEF). The PPEF was interpreted first by Nishida (1968) as the transmission of the magnetospheric convection electric field from high to low latitudes. Many experimental and theoretical studies of the prompt penetration of magnetospheric convection were made during the last decades (Vasyliunas, 1970; Senior and Blanc, 1984; Mazaudier et al., 1984; Spiro et al., 1988; Kikuchi et al., 1996; Kobea et al., 1998; Kobea et al., 2000; Peymirat et al., 2000; Mene et al., 2011). The DDEF is related to the transfer of thermal energy to the neutral gas via the Joule heating and impulses through the ion-neutral momentum transfer. The dissipation of the Joule heating by the auroral electrojet sets up gravity waves and equatorward thermospheric winds (the Hadley cell between the poles and the equator) at F-region altitudes (Testud and Vasseur, 1969; Richmond and Matsushita, 1975; Richmond and Robble, 1979). These storm winds extend from auroral zone to mid and low latitudes (Mazaudier et al., 1985) with a small return flow at the E-region altitudes around the equator (below about 120 km altitude). Blanc and Richmond (1980) made the first numerical simulation of the ionospheric dynamo. Many experimental and theoretical studies illustrated the characteristics of the ionospheric disturbance dynamo process (Fejer et al., 1983; Sastri, 1988; Abdu et al., 1997; Fambitakoye et al., 1990; Mazaudier an Venkateswaran, 1990; Fejer and Schierless, 1995; Richmond et al. 2003; Le Huy and Mazaudier , 2005; Le Huy and Mazaudier, 2008; Zaka et al., 2009; Zaka et al., 2010). The storm winds also lift the ionized regions. As a consequence, daytime increases occur in hmF2, in foF2, in total electron content (TEC) and the atmospheric composition changes globally (Jones, 1971; Jones and Rishbeth, 1971; Volland, 1979). The PPEF, the DDEF, and the storm winds modify the behavior of the equatorial ionosphere: the EIA, the PRE, the EEJ, and propitiate the occurrence of the EPB. They affect the Vertical Total Electron Content (VTEC), and the Rate of TEC Index (ROTI) as well as ionospheric F2 layer and geomagnetic variations.

In the framework of the International Heliophysical Year project (IHY/2005-2009) (http://www.unoosa.org/oosa/en/ourwork/psa/bssi/ihy2007.html), and the International Space Weather Initiative project (ISWI/2010-2012) (http://www.iswi-secretariat.org), a larger number of GPS stations were deployed all over Africa. This allowed the ionosphere research in Africa. Many ionosphere studies were made using the GPS data (Obrou et a., 2009; Ouattara et al., 2012; Bolaji et al., 2012; Bolaji et al., 2013; Oladipo et al., 2014; Bolaji et al., 2015) on the solar cycle and the seasonal behavior of TEC (Moeketsi et al., 2007; Ackah et al., 2011; Zoundi et al., 2012; Shimeis et al., 2014), and on geomagnetic storms (Shimeis et al., 2012; Adeniyi et al., 2014; Shimeis et al., 2015).

In this paper, we presented the day-to-day variability of VTEC and ROTI in October 2012 over the Asian, African, and American sectors of the Northern and Southern hemispheres. We focused on the 13 October 2012 case under the influence of a high-speed solar wind stream (HSSWS). A similar case was analyzed by Azzouzi et al. (2015), only in the European and African sectors. In this study, we extended our analysis to all longitude sector. We want to know whether the same type of solar event produces the same effect on the ionosphere in middle and low latitudes and determines the longitudinal extension. The GPS data were used to study the impact of a Coronal Mass Ejection (CME) and the impact of a HSSWS from a coronal hole on the VTEC and the ROTI which indicates the presence of irregularities in the ionosphere. Basu et al. (1999) showed that: "*the rate of change of TEC index (ROTI) that can be obtained from widely dispersed IGS stations performing two-frequency GPS satellite observations can be used, especially in the equatorial region, as an indicator of the presence of scintillation causing small-scale ionospheric irregularities*".

The second section of this paper is devoted to the data sets and data processing. The third section shows the results on the VTEC and the ROTI and the comparison between the 13 October 2012 case and the 14 October 2013 case presented by Azzouzi et al. (2015).Then we discussed the results in the fourth section and gave the conclusion in the fifth section.

2. Data set and data processing

2.1 Data sets

We analyzed the data in October 2012 focusing on the period of 12 to 17 October. The data of the Solar and Hemispheric Observatory (SOHO) satellite, (www.nasa.gov/mission_pages/soho/) and the website: www.space.weather.com were used to determine the solar sources (Coronal Mass Ejection (CME) and coronal hole). The observations of the Advanced Composition Explorer (ACE) satellite (http://omniweb.gsfc.nasa.gov/) provide solar wind parameters: the solar wind speed and the north-south (Bz) component of the Interplanetary Magnetic Field (IMF).

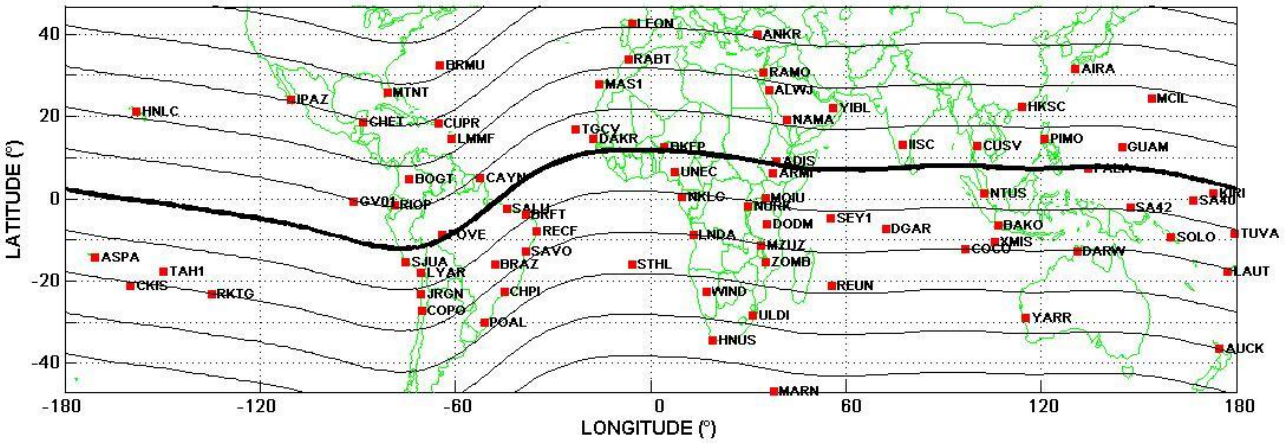

Figure 1. Location of the GPS stations used to make maps of ROTI.

The magnetic indices of SYM-H, AU, AL, AE, and Am/Km and the list of Storm Sudden Commencement (SSC) used in this study were extracted from the International Union of Geodesy and Geophysics (IUGG) website (http://isgi.latmos.ipsl.fr) (Mayaud, 1980; Menvielle et al., 2011). The Am/Km indices give an estimation of the global magnetic disturbances, just like Ap/Kp indices that are more often used. The Am/Km indices are the mean value of the K indices in 21 observatories over all the longitude sectors. There are 12 observatories in the Northern hemisphere and 9 in the Southern hemisphere. Ap/Kp indices are based only on 11 observatories; 9 in the Northern hemisphere and 2 in the Southern hemisphere. Am index is in nT and Km index is a number between 0 and 9.

Figure 1 presents the GPS network used to produce maps of ROTI. The GPS data were extracted from the websites: GPS Europe (http://www.epncb.oma.be/), the Scripps Orbit and Permanent Array Center (SOPAC) (http://sopac.ucsd.edu/), and the UNAVCO (http://www.unavco.org/), and the International GNSS Service (IGS) (http://igs.org/).

2.2 Data processing

VTEC

We used a standard procedure for processing GPS measurements given by Hoffmann-Wellenhof et al., (1992) and Schaer (1999) and for the conversion of slant TEC (STEC) to VTEC, we use the single layer mapping function (Schaer, 1999; see Azzouzi et al., 2015 for more details).

ROTI

We computed the ROT in units of TECU/min as follows:

$$ROT = \frac{STEC_{k+1} - STEC_k}{time_{k+1} - time_k} * 60 \qquad (1)$$

Where time (k), is a time during the day between 0 and 86400s and time (k+1) is the time 30 s later.

ROTI is then computed each 30s, by taking the standard deviation of ROT (Pi et al., 1997) over a period of 10-min and with a minimum of 10 points, i.e.

$$ROTI = \sqrt{\langle ROT^2 \rangle - \langle ROT \rangle^2} \qquad (2)$$

The ROTI is used to get information of irregularities in the F-region.

Maps of ROTI

The maps of ROTI are obtained by using 67 GPS stations located all over the globe in middle and lower latitudes (Figure 1). We used the ROTI each 30s and plot the ROTI when it is greater than 1.5 TECU/min.

We chose four arbitrary sectors longitudes:

Asia: 60^0-160^0E, number of stations 15
Pacific: 160^0-260^0E, number of stations: 14
America: 260^0-335^0E, number of stations: 18
Africa: 335^0-60^0E, number of stations: 20

The number of stations is balanced in areas (see Figure 1). However, it is not sufficient for the analysis of occurrence of the irregularities.

Percentage of irregularities occurrence expressed by ROTI

We computed the number of ROTI more than 1.5 TECU/min for 24 hours a day and obtained the number Nrot for each zone. For each day and each zone, we also computed the total number of ROTI values for each zone and obtained the number Ntot. The percentage of irregularities occurrence for each zone and each day is given by:

$$R = N_{rot} / N_{tot} \qquad (3)$$

3. Results

3.1 Global context of the 13 October 2012 case and the14 October 2013 case

In October 2012, three major solar events affected the Earth. A CME hit the Earth at 05:26UT on 8 October and the impact was seen as a SSC. After this CME, two HSSWSs related to coronal holes arrived in the evening (~19:00UT) on 9 October and in the afternoon (~17:00UT) on 13 October.

Figure 2 illustrates the variation of solar wind parameters and magnetic indices between 7 and 22 October: solar wind speed in km/s, the Bz component of the IMF, the SYM-H indices, and the AU and AL

indices (from the top panel to the bottom panel). The SSC is indicated by the vertical red line in the SYM-H panel. On the top panel, the arrivals of the HSSWSs are indicated by two red arrows. On 17 and 18 October, there were also increases of the solar wind speed which were not reported as related to coronal holes. On 8 October, the IMF Bz was southward when the CME hit the Earth (~-5 nT) and decreased after the shock (-15nT). Then it increased and turned northward (+ 10 nT) around 12:00UT and turned southward (~-15 nT) around 18:00UT again. Large variations of SYM-H and AL indices were associated to the southward excursions of the IMF Bz. On October 9 when the first HSSWS arrived in the evening (~22:00UT), the IMF Bz was oscillating and then became northward (+10 nT) around 00:00UT. The SYM-H was in a recovery phase (~10 nT). SYM-H and AL showed small variations just before 00:00UT associated to this HSSWS. On 13 October, the second HSSWS arrived also during the recovery phase of a storm around ~16:00UT. This storm started around 00:00UT on 12 October with southward turning of the IMF Bz. In this case, the HSSWS was associated to a decrease of SYM-H from ~-45 nT (~16:00UT) to ~-70 nT (~18:00UT) and to an increase of the AL index (~1000nT). The solar wind speed reached 570km/s around 17:00UT. The effect of this HSSWS was stronger than the effects of the first HSSWS. Because both the SYM-H and the IMF Bz were stronger than those of the first HSSWS event. During the increases of solar wind speed on 17 and 18 October, there was no large variation of the SYM-H and AL indices.

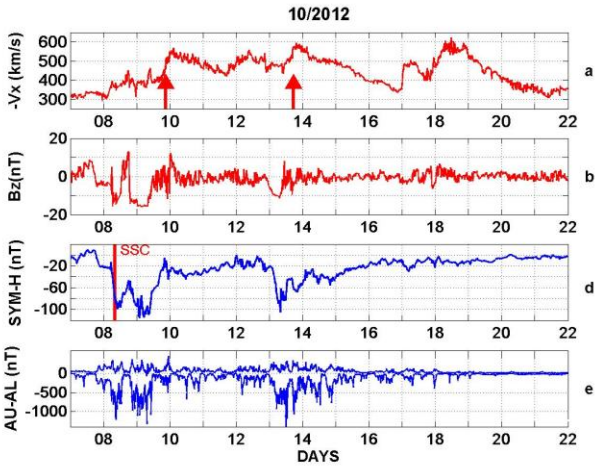

Figure 2. Variations of solar wind parameters (solar wind speed and IMF Bz) and geomagnetic indices (SYM-H, AU, and AL) for the period between 7 and 22 October 2012. Two arrows show arrivals of HSSWSs.

In October 2012 and 2013, the complete disappearance of the scintillations on the GPS signal was observed over the whole Africa only on 13 October 2012 and on 14 October 2013. We compared these two events to understand the similarity between them.

Table 1 shows the characteristics of the solar wind speed, Dst and AE indices on 8, 9, 13, 17, and 18 October 2012 and on 14 October 2013 (Azzouzi et al., 2015). The table presents the AE index more than >~300 nT for several hours both on 13 October 2012 and on 14 October 2013.

Figure 3 shows the convection maps by the Super Dual Auroral Radar Network (SuperDARN) around 19:00UT on 8, 9, 13, 17, and 18 October 2012 and on 14 October 2013. The largest convection cells were observed on 13 October 2012 and 14 October 2013. The largest cells of convection observed on these two days can produce large electric fields (the PPEF and the DDEF). These electric fields were able to generate disturbances of the equatorial VTEC and ROTI.

Table 2 gives the values of the cross polar cap potential and of the latitudinal extension of the convection cells between 16:50UT and 19:00UT. The 13 October 2012 case is similar to the 14 October 2013 one concerning the pattern of the auroral zone. The largest cross polar cap potential (49kV to 82 kV) and the largest extension of the convection cells toward mid latitudes (61^0 to 50^0N) were observed on 13 October 2012 and 14 October 2013. The latitudinal extension of the convection cells was between 64^0 and 72^0 N and the cross polar cap potential was between 23kV and 66kV for all other days.

3.2 Day-to-day variability of VTEC of the 13 October 2012 case

In the following sections, we analyzed global scale characteristics of the VTEC for this event. Figure 4 shows the variation of the Am index in October 2012. Geomagnetic activity was high in the first two weeks in October 2012 and became low (Am index less than 14 nT) in the rest of the month. The Am index on 1 October was 38 nT due to the impact of a CME arrived at the Earth on 30 September. When the first HSSWS arrived on 9 October, the Am index increased and reached 63nT. The Am index increased from 23 nT to 61 nT associated with the second HSSWS on 13 October.

Figures 5a and 5b show the day-to-day variation of VTEC, observed in a chain of GPS stations of the Northern and Southern hemispheres in the Europe and East African sectors. The left panels are for the Northern hemisphere and the right panels are for the Southern hemisphere. The panels in the figures are aligned from top to bottom in order of decreasing latitudes. Figure 5a shows VTEC in high and middle latitudes and Figure 5b is that in middle and equatorial latitudes. The red rectangles indicate the period around 13 October and the pink curves represent the solar index (F10.7). The decrease associated with the second HSSWS varied in each station. We made similar figures for the Asian, American and West African sectors. They shows similar variations. According to Figures 5a and 5b, amplitudes of VTEC were smaller (~0-15 TECU) during the beginning of the month and were larger (~16-31 TECU) in the end of the month at all the GPS stations in high and middle latitudes of the Northern hemisphere (VARS, VLNS, MIKL, ANKR, NICO, and RASH) and of the

Table 1. Solar wind speed and Dst and AE indices, on 8, 9, 13, 17, and 18 October 2012 and on 14 October 2012.

Event	Solar wind speed	Dst index at 19:00UT	AE indices between 18:00UT and 19:00UT
CME at 05:26UT on 8 October 2012	~300 km/s at 03:00UT ~390 km/s at 05:30UT	-70 nT	less than 100 nT from 14:00UT to 19:00UT
coronal hole on 9 October 2012	~400 km/s at 19:00UT ~580 km/s at 24:00UT	-45 nT	~500 nT at 19:00UT less than 200nT from 12:00UT to 18:00UT
coronal hole on 13 October 2012	~450 km/s at 10:00UT ~600 km/s at 16:00UT	-62 nT	~1300 nT at 19:00UT ~300 nT for several hours before 19:00UT
17 October 2012	~360 km/s at 00:00UT ~490 km/s at 02:00UT	-4 nT	less than100 nT for all the day
17-18 October 2012	~400 km/s at 21:00UT on 17 ~600 km/s at 10:00UT on 18	-9 nT	less than 100 nT for all the day
14 October 14 2013	~330 km/s at 07:30UT ~ 460km/s between 12:00UT and 24:00UT	-22 nT	~1000 nT at 19:00UT less than 300 nT for several hours before 19:00UT

Table 2. Polar cap potential and latitudinal extension of the convection cells obtained by the SuperDARN observation on 8, 9, 13, 17, and 18 October 2012 and on 14 October 2012.

Time	14 October 2013	13 October 2012	8 October 2012	9 October 2012	17 October 2012	18 October 2012
16:50UT 16:52UT	82 kV 560	49 kV 590	18 kV 690	56 kV 680	32 kV 700	40 kV 640
17:00UT 17:02UT	78kV 560	63kV 610	32kV 680	53kV 670	32kV 650	44kV 640
17:50UT 17:52UT	76kV 530	74kV 500	18kV 690	46kV 680	29kV 700	25kV 700
18:00UT 18:82UT	71kV 550	67kV 500	27kV 680	54kV 680	19kV 710	33kV 720
18:50UT 18:52UT	69kV 540	62kV 550	47kV 680	45kV 640	15kV 710	34kV 690
19:00UT 19*02UT	65kV 540	63kV 550	66kV 680	62kV 640	23kV 700	41kV 680

Southern hemisphere (SYOG, MARN, SCOT, ZOMB, MZUZ, and DODM). In low latitudes of both the hemispheres (NAMA and ADIS in the Northern hemisphere and MAL2 and MOIU in the Southern hemisphere), there was no such a large difference in amplitudes of VTEC. The GPS stations in high and middle latitudes exhibited the same behavior: decreases of the VTEC from 1 to 7 October and increases of the VTEC from 8 to 14 October.

Table 3 shows the fluctuations of VTEC greater than 10 TECU. In high latitudes (VARS in Norway and SYOG in Antarctic) of both the hemispheres, the VTEC was lowest with many small fluctuations from 8 to 14 October. In the mid latitudes stations of the Northern hemisphere (MIKL, ANKR, NICO, and RASH), the same patterns were observed. The VTEC increased associated with the arrival of the CME on 8 October and then increased. It increased again associated with the arrival of the second HSSWS on 13 October.

The day of the decrease of the VTEC is different from one station to another (8, 9 or 10 October 2012). At ANKR and NICO, the largest amplitude of VTEC in October was observed on 13 October. In the Southern hemisphere, the same pattern was observed at the mid latitudes stations (MARN, SCOT, ZOMB, MZUZ, and DODM): 1) Increase of VTEC on 8 October, was larger than 10 TECU at MARN and SCOT and was less at ZOMB, MZUZ, and DODM, 2) Decrease of VTEC on 9 and 10 or 11 October and increase until 13 or 14 October were observed at all the stations. At MARN in the Southern hemisphere, the largest increase of VTEC was observed on 8 October. In the equatorial stations of the Northern and Southern hemispheres (NAMA in Saudi Arabia and MAL2 and MOIU in Kenya), we observed large fluctuations of VTEC, with amplitude comparable to other fluctuations during the same month when there was no solar disturbance, and therefore it is difficult to find the impact of the solar events. We can see the disturbance due to the impact of solar event when they were larger than the day-to-day variability. In the present case, the impact of the disturbance was not detectable at the equatorial stations. At ADIS in Ethiopia, there were no large fluctuation of VTEC and the VTEC increased slowly from 5 to 15 October.

Table 3. Latitudinal variations of VTEC in the European and Eastern African sectors.

GPS station in the Northern hemisphere	**VTEC variation more than 10 TECU**	**GPS station in the Southern hemisphere**	**VTEC variation more than 10 TECU**
VARS, Norway	small with fluctuations from 8 to 15 October	SYOG, Antarctic	small with fluctuations from 8 to 15 October
VLNS, Estonia	small from 8 to 14 October decrease of ~-10 TECU from 8 to 9 October increase of +15 TECU from 10 to 13 October	MARN, Islands Marion	increase of ~+20 TECU on 8 October decrease of ~-30 TECU on 9 October increase of ~+15 TECU on 13 October
MIKL, Ukraine	increase of ~+10 TECU on 8 October decrease of ~-15 TECU from 9 to 10 October increase of ~+15 TECU from 11 to 13 October	SCOT, South Africa	increase of ~+15 TECU on 8 October decrease of ~-20 TECU from 8 to 10 October increase of ~+20 TECU from 10 to 14 October
ANKR, Turkey	increase of ~+15 TECU on 8 October decrease of ~-15 TECU from 9 to 11 October increase of ~+20 TECU from 12 to 13 October	ZOMB, Malawi	decrease of ~-10 TECU from 9 to 10 October increase of ~+15 TECU 10 to 14 October
NICO, Cyprus	increase of ~+15 TECU on 8 October decrease of ~-15 TECU from 8 to 11 October increase of ~+20 TECU on 13 October	MZUZ, Zambia	decrease of ~-10 TECU from 8 to 10 October increase of ~+20 TECU from 10 to 14 October
RASH Israel	increase of ~+10 TECU on 8 October decrease of ~-15 from 8 to 10 October increase of ~+20 TECU from 11 to 13 October	DODM, Tanzania	decrease of ~-15 TECU from 9 to 10 October increase of ~+20 TECU from 12 to 14 October
NAMA, Saudi Arabia	decrease of ~-20 TECU from 11 to 12 October increase of ~+20 TECU from 12 to 13 October	MAL2, Kenya	increase of ~+10 TECU on 8 October decrease of ~-20 TECU on 11 October decrease of ~-20 TECU on 13 October
ADIS, Ethiopia	slow increase from 8 to 15 October	MOIU, Kenya	increase of ~+10 TECU on 11 October increase of ~+15 TECU on 13 October

3.3 Planetary study of ROTI on the 13 October 2012 case

Figure 6 presents the ROTI maps obtained from 67 GPS stations for the period from 7 to 22 October 2012. We used the ROTI each 30 seconds and plotted the ROTI greater than 1.5 TECU/min: occurrence of irregularities as red points. The calculation of ROTI is described in Section 2. The occurrence of irregularities was strongest in the American sector (except on 7 and 11 October 2012) and was weakest in the Asian sector in this period. The occurrence of irregularities increased in the Pacific sector during geomagnetic storms on 8 and 13 October. The occurrence of irregularities disappeared across Africa on 13 October and remained low on 14 October.

Figure 7 shows the percentage of ROTI above the threshold of 1.5 TECU/min. They were calculated following equation 3 in Section 2. The data are organized according to four areas of arbitrary longitudes: Africa between 335°E and <60°E, Asia between 60° and 160°E, Pacific between 160° and 260°E, and America between 260° and 335°E. The percentages are lower than 5% because irregularities are mainly observed only after 18 LT and for a more limited time slot. This figure shows that the occurrence of irregularities was observed in the Pacific sector (green curve) only during the two storms on 8 and 13 October. In the Asian sector (blue line), there were fewer occurrences of irregularities than in the African and American sectors.

In the African sector, the occurrence of irregularities decreased from 6 to 13 October (except a peak on 12 October). On 13 October, the occurrence became the minimum and no irregularity was observed. Then it increased and became its maximum on 19 October. After its maximum, it decreased with some fluctuations. The occurrence of irregularities in the African sector was less than other longitude sectors from 7 to 14 October except in the Pacific sector on 12 October.

In the American sector, the occurrence of irregularities decreased from 1 to 7 October. There was a peak on 9 October. The occurrence increased and became a maximum on 16 October. It remained above 2% level after 16 October.

Figure 8 shows the VTEC and ROTI observed at some specific GPS stations NKLG and DAKR in Africa (top panels), at GUAM in Asia (bottom left panel) and BRFT in Brazil (bottom right panel). On each panel, the VTEC variations (red curves) are superimposed to the ROTI (blue curves) for the period from 11 to 17 October.

The x-axis shows local time between 18 LT and 24LT. This figure shows no depletion of VTEC (signature of the EPB) and no variation of the ROTI at NKLG on 13 and 14 October, at DAKR on 13 October, and at GUAM on 12 and 15 October. We used PseudoRandom Noise (PRN) #7 at NKLG, PRN#4 at BRFT and at DAKR, and PRN#26 at GUAM because of visibility of them.

At BRFT on 13 October, the ROTI was zero all the night except for 20 minutes before 21:00LT. This figure (as Figures 5 and 6) shows that the lowest level of ROTI (i.e. scintillations) was observed at GUAM in the Asian sector.

We selected four very distant geographical positions (NKLG, DAKR, BRFT, and GUAM). It is not possible to see the same satellite on these 4 stations at the same moment. We chose the GPS satellites which passed closer to each station for the calculation of the VTEC and ROTI. This analysis using a few GPS satellites and several stations showed that increase of ROTI seems to be associated with decrease of VTEC.

The second HSSWS which hit the Earth on 13 produced the disappearance of scintillations of the GPS signal. It is interesting to compare this case with the normal behavior during magnetic quiet days (Figure 9) in order to consider the day-to-day variability.

Figure 9 shows the track of ionospheric pierce points (taken at 450 km) of the satellite PRN#07 (used the plot of Figure 8) for several GPS stations near NKLG on 15 October. Trajectories of the satellite are shown in black and the locations of an EPB are shown in red on them. The trajectories crossed almost perpendicularly the magnetic equator (dip = 0 in green). The EPB was located below the inclination line 10 magnetic south. At the BRGL station (Angola) in further south from NKLG, there was no observation of the EPB. This can be interpreted by the fact that the satellite was too far south between 19:00UT and 20:00UT and could not see the area with the irregularities of the EPB. On 15 October, the spatial extent of the EPB was between 0 and -10 degrees in geomagnetic latitude.

4. Discussion

In this paper, we analyzed the ionospheric condition in October 2012 and focused on the 13 October 2012 case characterized by an increase of the solar wind speed around 16:00UT by the second HSSWS. This case is similar to the 14 October 2013 case: the arrival of the HSSWS near the Earth during daytime (Azzouzi et al., 2015). We first discussed the global context and made a comparison of the two specific cases.

4.1 Global context

We analyzed the planetary-scale VTEC and presented only the results of the Europe and Eastern African latitudinal chain (Figures 5a and 5b), because the results for the other latitudinal chains of the West African sector, of the Asian sector, and of the East and West American sector showed similar variations. In mid latitudes, the VTEC increased on 8 October, at the arrival of the CME, in the Northern and Southern hemispheres. Such an increase was found by Shimeis et al. (2012) at the Northern crest of ionization in Egypt and Azzouzi et al. (2015) in different mid latitudes of the Northern hemisphere. The increase of VTEC with the arrival of the CME is interpreted as due the Prompt Penetration Electric Field (PPEF) (Nishida et al., 1966; Nishida, 1968; Vasyliunas, 1970). In our study, the observed variations in mid latitudes were similar both in the Northern and Southern hemispheres. It was not the case for Shimeis et al. (2015); they found a large asymmetry between the Northern and Southern hemisphere over Africa when they studied the period between 5 and 10 April 2010. On the day after the CME, VTEC always decreased in mid latitudes. This is interpreted by the effect of the Ionospheric Disturbance Dynamo (Blanc and Richmond, 1980). Such decreases of electron density were observed on density of the F2 layer by Sastri (1988) and on VTEC by Shimeis et al (2012; 2015) and Azzouzi et. (2015) recently. A rapid heating and expansion of the atmosphere in high latitudes result in pressure gradients. This pressure gradients in turn, modify the global thermospheric circulation, and produce equatorward winds (Richmond and Matsushita, 1975; Richmond and Roble, 1979). These equatorward winds by a storm produce the composition changes to middle latitudes and cause a reduction in the level of ionization (Yizengaw et al., 2005).

In equatorial latitudes, there was no clear signature of the arrival of the CME (bottom panels of Figure 5b). In high latitudes (top panels of Figure 5a), the regular variations of VTEC were hidden by fluctuations of VTEC associated to the CME.

We presented the maps of ROTI in Figure 6 and the percentage of irregularities in the four longitude sectors (the Asian, African, Pacific, and American sectors) in Figure 7. These two figures show the complete disappearance of irregularities over the whole Africa on 13 October. These figures highlight also the strong asymmetry of ROTI between the American and the Asian sectors. The occurrence of irregularities in the Pacific sector was observed only on 8 and 13 October. Su et al. (2007) analyzed the equatorial irregularities with the ROCSAT-1 at the 600km topside ionosphere from March 1999 to June 2006; their conclusions are that the irregularities are mostly variable in all the longitude sectors. This means that we cannot draw general conclusions from these maps. Su et al. (2007) concluded: '*Furthermore, the seasonal/longitudinal variations of quiet time post sunset vertical drift velocities are found to track closely with the seasonal/longitudinal variation of irregularity occurrences.*' The vertical drift is the main driver of the irregularities.

Chatterjee and Chakraborty (2013) noticed that the locations of observatories with respect to the post-sunset resurgence peak of the EIA seem to play dominant role indicating the severity of irregularities. In Figures 5a and 5b, the VTEC was lowest during the geomagnetically disturbed period between 8 and 14 October (Figure 4). Figure 7 shows similar tendency.

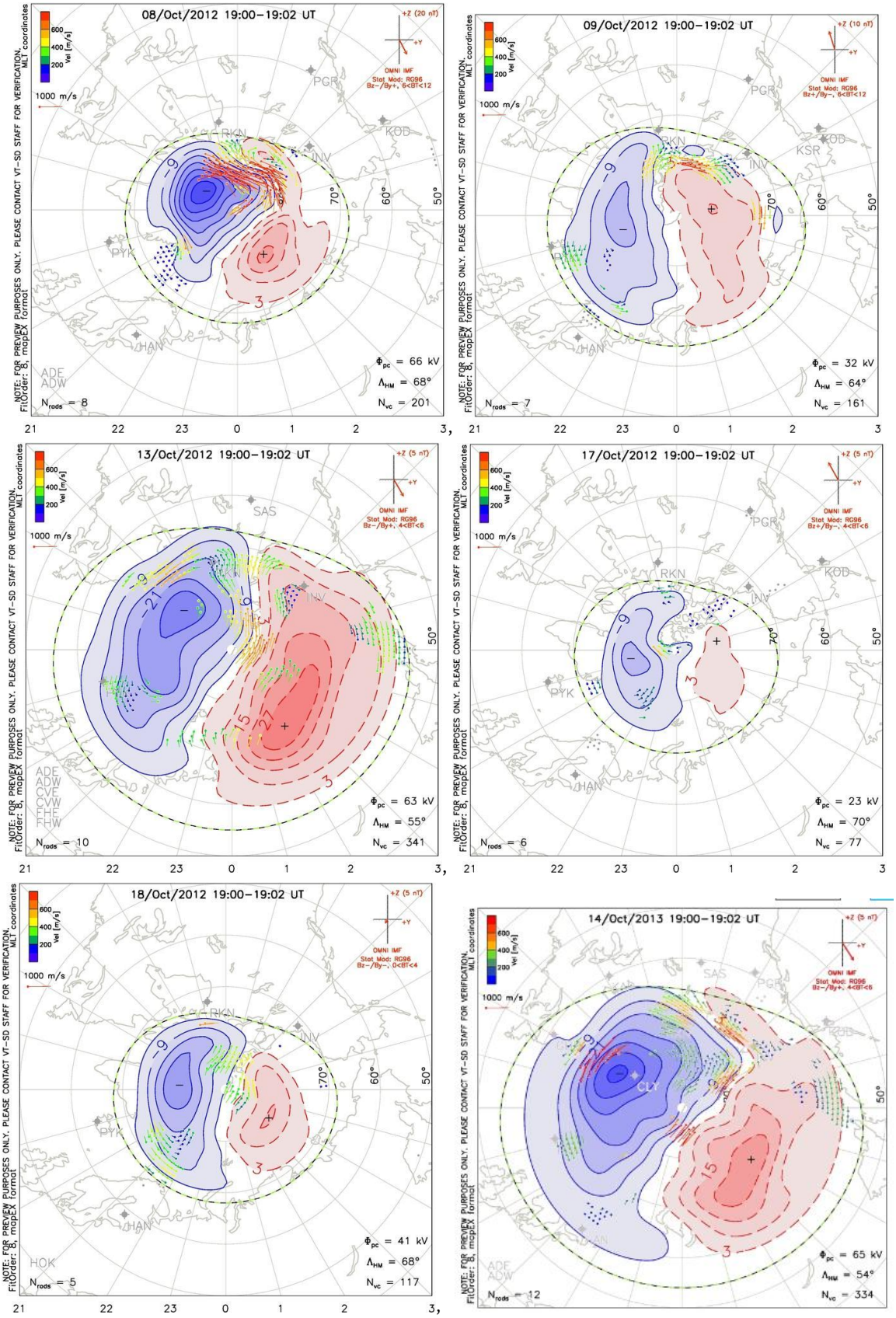

Figure 3. Convection maps by the SuperDARN at 19:00UT on 9, 13, 17, and 18 October 2012 and on 14 October 2013.

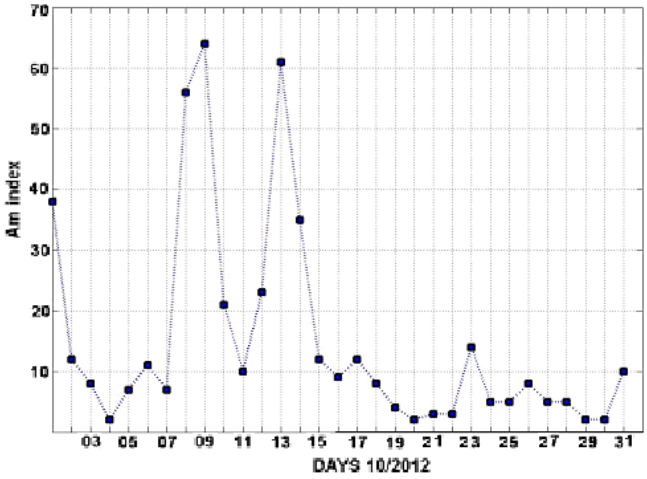

Figure 4. Am indices in October 2012.

The occurrence of irregularities was lowest during the geomagnetically disturbed period. Because the equatorial electric field is changed through variation of the general thermospheric circulation by the Joule heating in the auroral zone during the geomagnetically disturbed period. The plasma is moved down to lower altitude by a westward electric field due to the disturbance dynamo (Blanc and Richmond, 1980) associated to the perturbation of neutral winds. In lower altitude, electron density decreases by increase of recombination rate (Figures 5a and 5b).

4.2 Comparison between the 13 October 2012 case and the 14 October 2013 case

The 13 October 2012 case is similar to the 14 October 2013 case (Azzouzi et al., 2015). In the beginning of this paper, we showed the similarities of these cases. Both cases exhibited a large variation of the AE index (>~1000 nT) in the evening (~19:00UT). The AE index is used to determine the Joule heating (Ahn et al., 1983; Baumjohan and Kamide, 1984) and it is known that the Joule heating is the major source of disturbance of the thermospheric wind during magnetic storms. These events also exhibited a large extension of the convection cells from auroral latitudes toward mid latitudes (see the convection maps by the SuperDARN in Figure 3). Table 2, which gives the polar cap potential and the latitudinal extension of convection cells, shows that these two events presented the similar values between 17:00UT and 19:00UT and were different from the other events on 8, 9, 17, and 18 October 2012.

On 13 October 2012, the ROTI (Figure 8) was zero at the GPS stations: NKLG (LT=0U +1, Gabon in Central Africa) and DAKR (LT=0UT-1, Senegal in West Africa). The same behavior was observed on 14 October 2013 (see Figure 5 in Azzouzi et al. (2015)).The ROTI at BRFT (Brazil) was not analyzed in Azzouzi et al., 2015. The fact that the ROTI was zero suggested the absence of ionospheric irregularities. The irregularities are associated to the PRE (Kelley, 2009), which causes a strong upward vertical drift (Vz), and generates irregularities. If the Vz is reduced, there is inhibition of the EPB. Carter et al., (2014), using the Thermosphere Ionosphere Electrodynamic General Circulation Model (TIE-GCM) model found that the model produces the larger Vz (by 5 m/s) on EPB days compared to non-EPB days at the time of the PRE.

The observation data in Figure 8 show that the impact of the HSSWS occurred at local time between 0UT+1 (NKLG) and 0UT-3 (BRFT). In the East Africa (Figure 6), there is a low value of ROTI on 13 October 2012, therefore, we can conclude that the impact of this disturbance was regional, and inhibited irregularities in all the stations with local time between 0UT+3 to 0UT-3. On Figure 9, we show the extension of the EPB observed with the ROTI on 15 October 2012, a magnetic quiet day. Previously, Santos et al. (2012) found similar results. They found a strong longitudinal difference in ionospheric responses, over Fortaleza (Brazil) and Jicamarca (Peru), during the January 2005 geomagnetic storm, with the total suppression of the PRE over Fortaleza and no simultaneous effect over Jicamarca. Abdu et al., (2009), first presented the case of removal of the PRE and spread F, by an electric field disturbance due to the PPEF and more recently, Azzouzi et al. (2015) presented a case of removal of the PRE and spread F, by the DDEF.

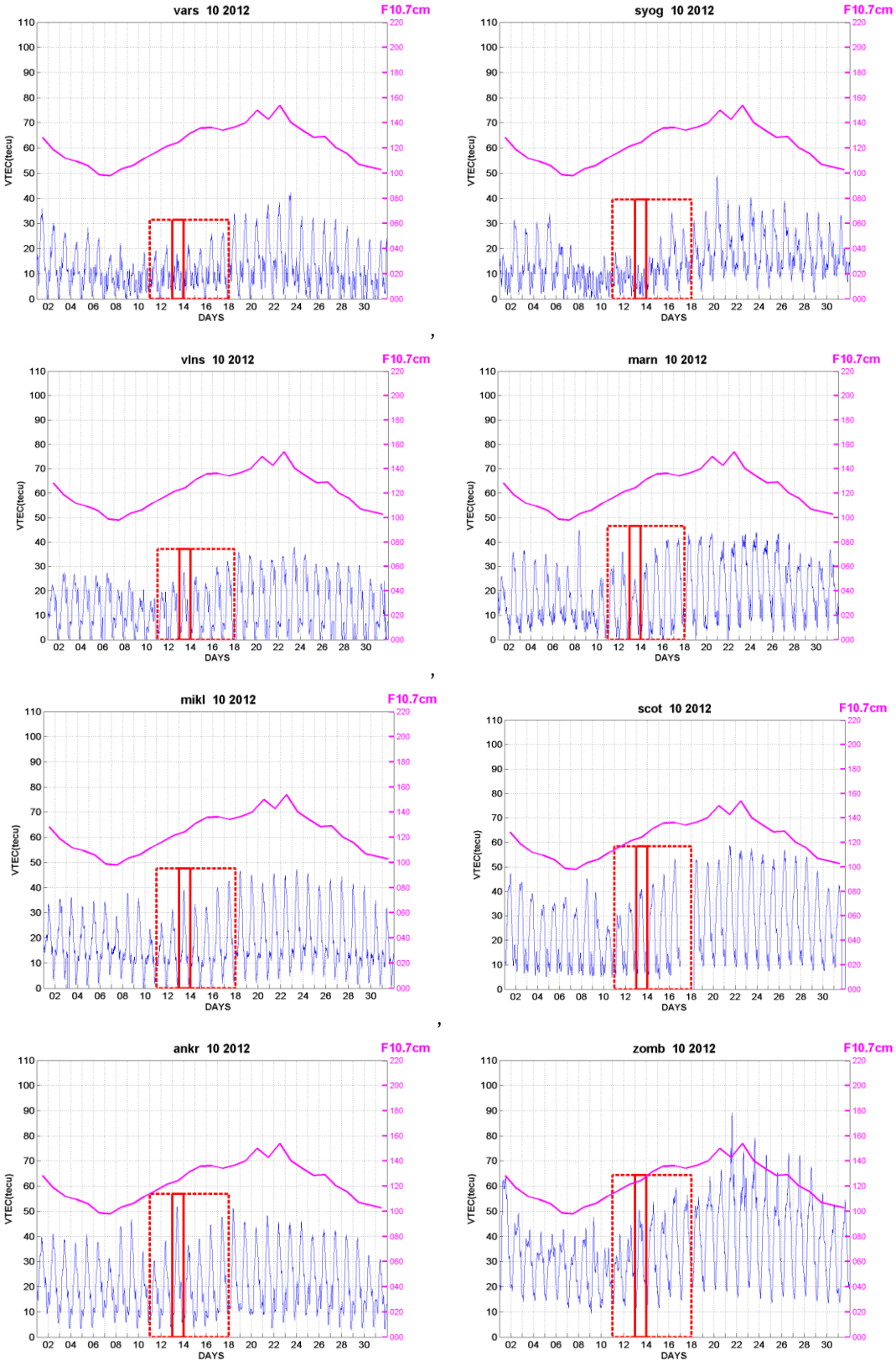

Figure 5a. VTEC observed in high and middle latitudes in October 2012. The left panels show the stations in the Northern hemisphere and the left panels shows the stations in the Southern hemisphere.

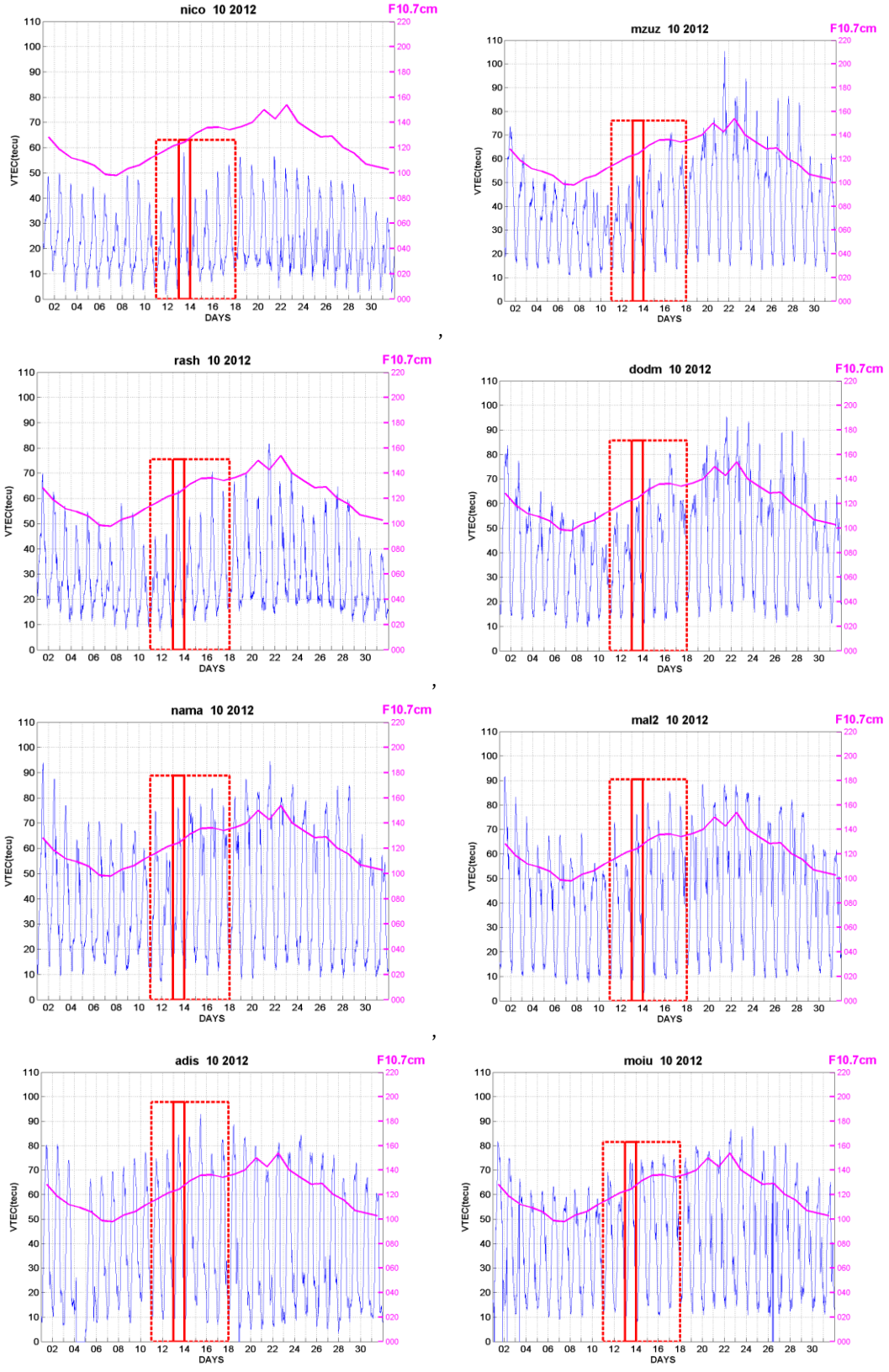

Figure 5b. VTEC observed in middle and low latitudes in October 2012. The left panels show the stations in the Northern hemisphere and the left panels shows the stations in the Southern hemisphere.

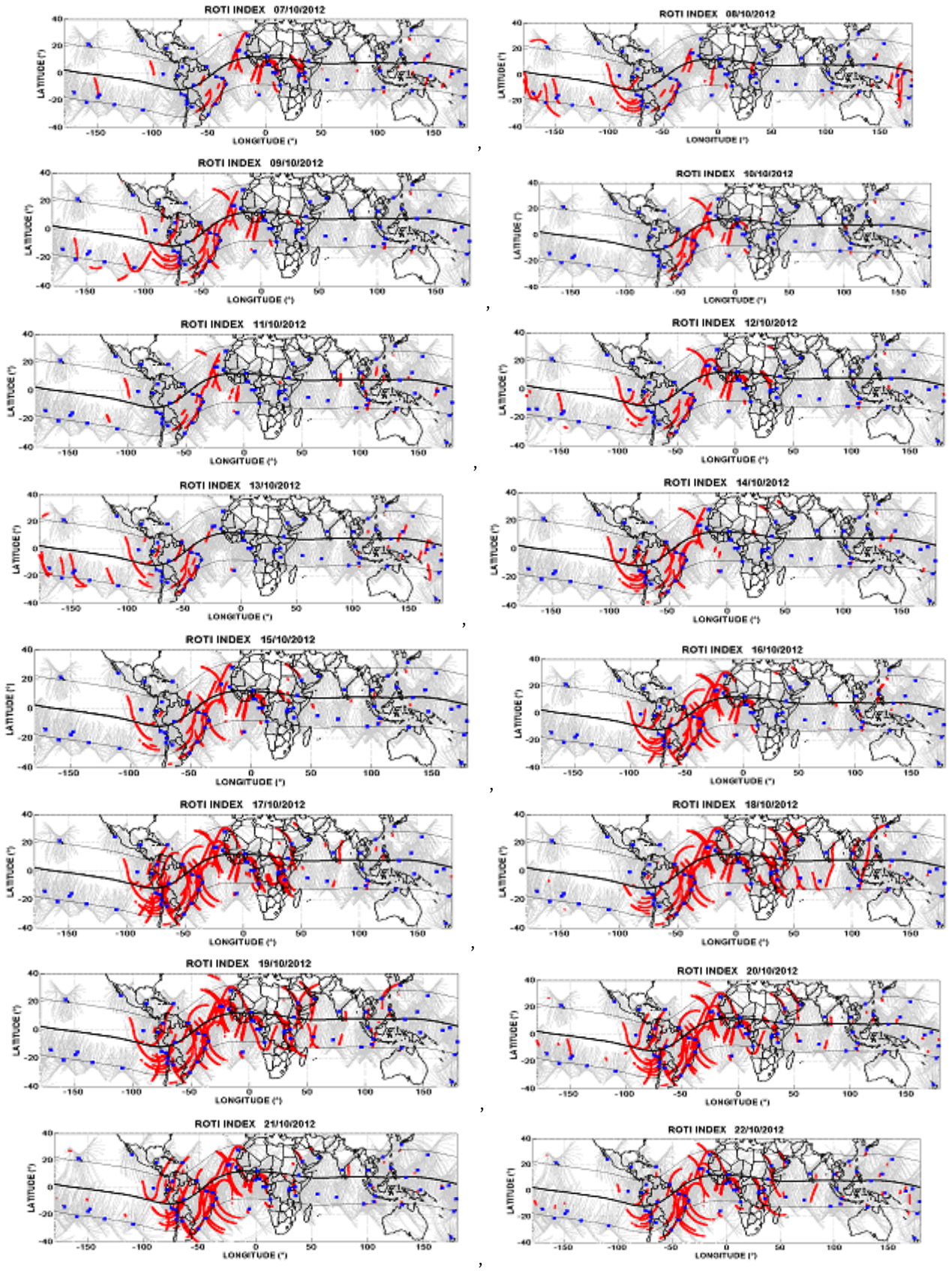

Figure 6. Maps of ionospheric irregularities identified by ROTI more than 1.5 TECU/min. calculated by the GPS data between 7 and 22 October 2012.

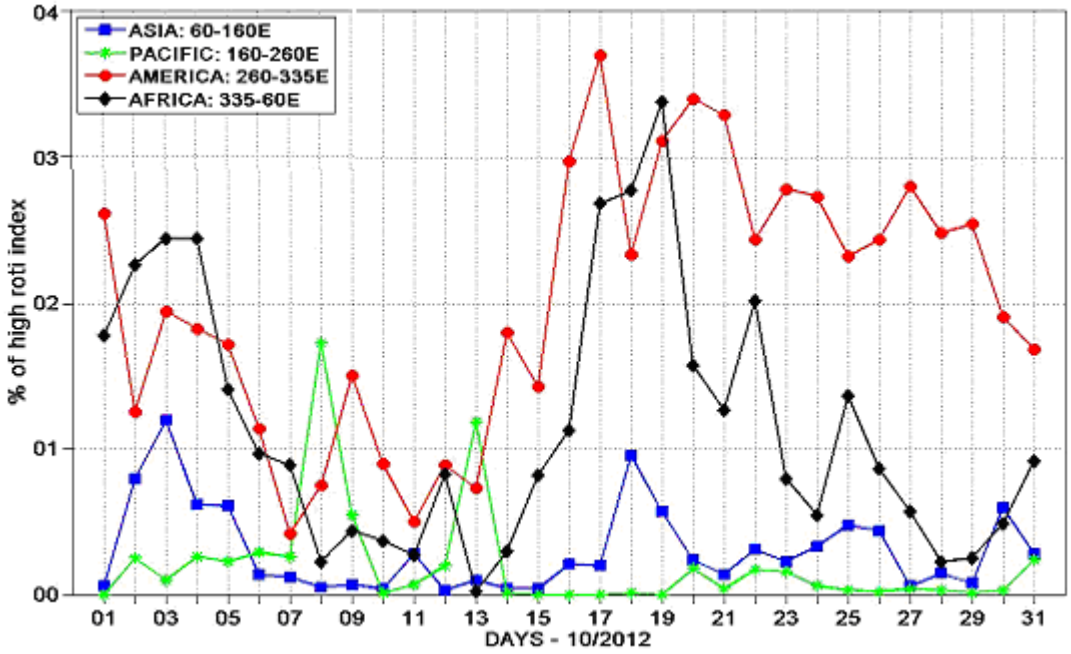

Figure 7. Percentage of occurrence of irregularities in the African, Asian, American, and Pacific longitude sectors.

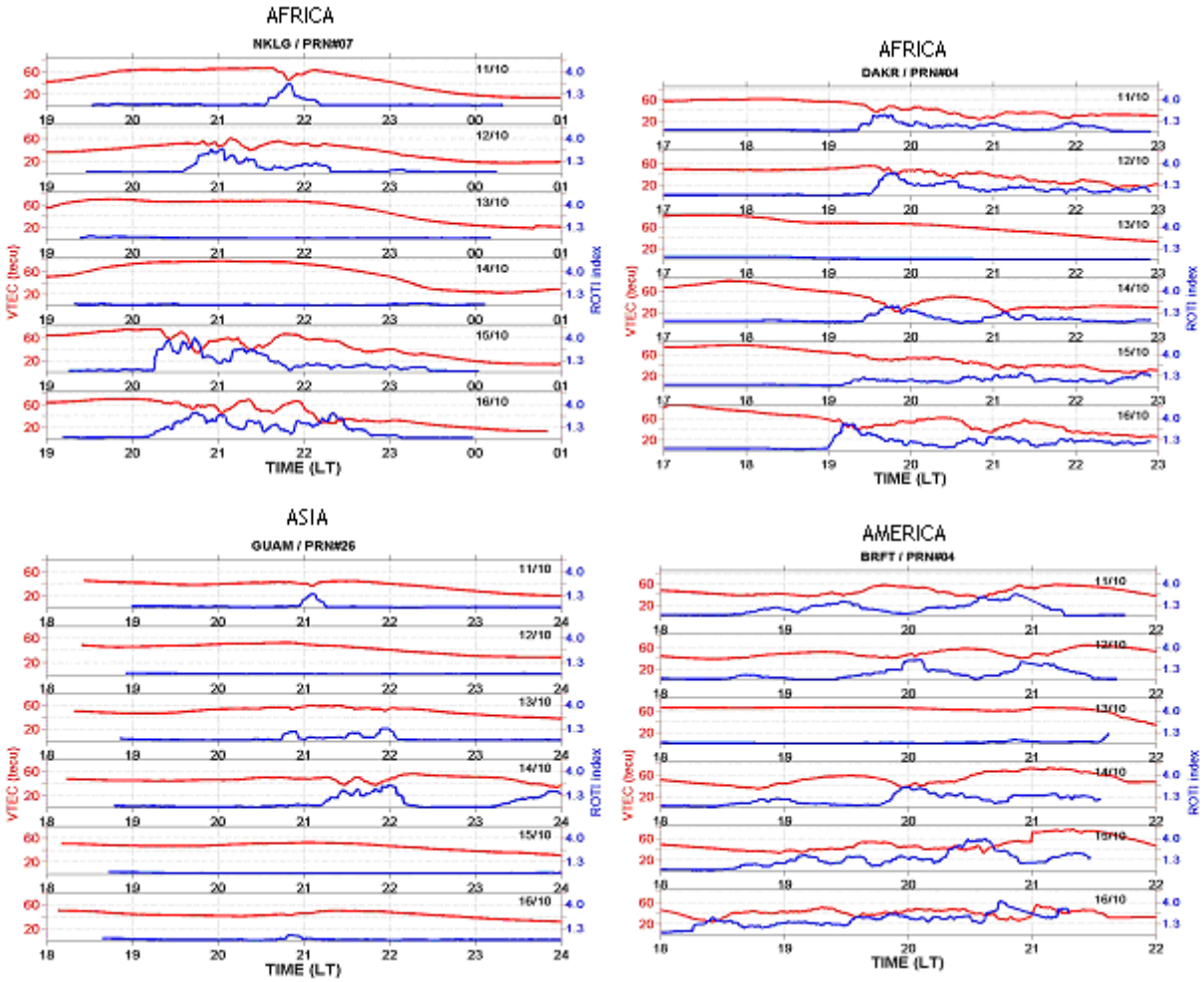

Figure 8. TEC and ROTI observed in the African, Asian, and American sectors for the period from 11 to 17 October.

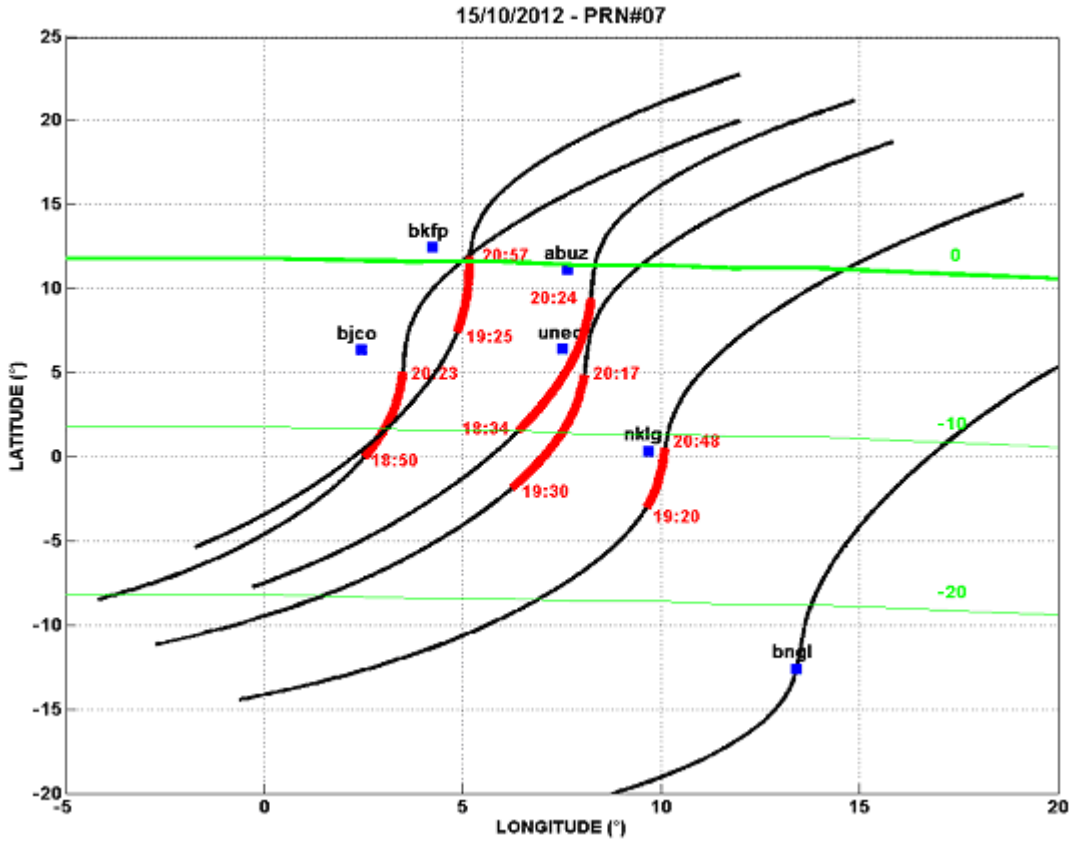

Figure 9. An example of extension of a plasma bubble detected by the TEC observations on 15 October 2012 near the equator of Africa.

Summary and conclusion

In this paper, we analyzed the ionospheric phenomenon in October 2012 and more particularly the case on 13 October when ionospheric irregularities (estimated by the ROTI) disappeared over whole Africa.

We considered the phenomenon of the Northern and Southern hemispheres in the Asian, African, and American longitude sectors and found the following results:

- ✓ The GPS stations in high and middle latitudes exhibited the following behavior: a decrease of the VTEC between 1 and 13 October and then an increase of the VTEC on 14 October. On this global variation, the fluctuations of the VTEC due to the CME and the HSSWSs from coronal holes were superimposed.
- ✓ The effect of the CME arrived on 8 October was clearly identified in middle and low latitudes of both hemispheres by an increase of the VTEC after its impact and a decrease of VTEC for several days. The increase of VTEC is interpreted as due to the physical process of the PPEF. And the decrease of VTEC is interpreted as due to the DDEF.
- ✓ In equatorial latitudes, no clear signature of the impact of the CME on the VTEC was observed.
- ✓ The impact of the CME on the VTEC was rather similar in the three different longitude sectors.
- ✓ The impact of the CME on the VTEC was stronger in the Northern hemisphere than in the Southern hemisphere.
- ✓ The ROTI associated with the disturbance by the CME was greater in the American sector than in the African and Asian sectors.
- ✓ The impact of the HSSWS arriving in the afternoon on 13 October was identified in the ROTI. The ROTI was zero over all Africa and was almost zero over Eastern America. These observations highlight the impact of the HSSWS was regional and affected the stations with local time LT=UT+3 and UT-3 corresponding to a longitude sector 3150E to 450E. This case is similar to the case studied by Azzouzi et al. (2015) over West Africa and can be interpreted by the effect of the DDEF which affected the PRE and inhibited the ionospheric irregularities. The novelty of this paper (comparing to the work of Azzouzi et al., (2015)) is that we analyzed the 13 October 2012 event in the global context and found the longitude sector more impacted by the HSSWS. The signature of the event was observed by the VTEC and ROTI data.

As our future work, we will analyze the impact of HSSWS in the middle and low latitudes in different phases of the solar cycle and model the results.

Acknowledgment

The authors thank all the providers of the GPS data of the IGS and the UNAVCO networks. The authors thank the SuperDARN for the maps of convection. Our sincere thanks go to all members of the LPP/Polytechnique/UPMC/CNRS, Telecom Bretagne-Brest University, the Ecole Mohammadia d'Ingénieurs (EMI)/Université Mohammed V Agdal Rabat-University, and the ICTP -International Centre for Theoretical Physics, the for their ceaseless support. This work was supported by a part of the JSPS Core-to-Core Program (B. Asia-Africa Science Platforms), Formation of Preliminary Center for Capacity Building for Space Weather Research. This is IPGP contribution n.3719.

References

Abdu, M. A., de Medeiros, R. T., Sobral, J. H. A., and Bittencourt, J. A.: 1983, J. Geophys. Res., 88(A11), 9197.

Abdu, M. A., Kherani, E. A., Batista, I. S., and Sobral, J. H. A.: 2009, Geophys. Res. Lett., 36, L19103, doi:10.1029/2009GL039919.

Ackah, J-B, Obrou, O. K., Zaka, Z., Mene, M. N., and Groves, K.: 2011, Sun and Geosphere, 6 (1), 27.

Adeniyi, J. O. , Doherty, P. H., Oladipo, O., and Bolaji, O. S.: 2014, Radio Sci., 49, doi:10.1002/2014RS005404.

Ahn, B., Akasofu, S. I., and Kamide, Y.: 1983, J. Geophys. Res., 88, 6275.

Appleton, E.: 1946, Nature, 157, 691.

Azzouzi, I., Migoya-Orué, Y., Amory Mazaudier, C., Fleury, R., Radicella, S., and Touzani, A.: 2015, Adv. Space Res., 56(9), 2040, doi:10.1016/j.asr.2015.06.010.

Basu, S., and Basu, S.: 1981, J. Atmos. Sol. Terr. Phys., 43 (5/6), 473.

Basu, S., Groves, K. M., Quinn, J. M., and Doherty, P.: 1999, J. Atmos. Sol. Terr. Phys., 61, 1219.

Baumjohan, W., and Kamide, Y.:1984, J. Geophys. Res., 89, 383.

Blanc, M., and Richmond, A.D.: 1980, J. Geophys. Res., 85(A4), 1669.

Bolaji, O. S., Adeniyi, J. O., Radicella, S. M., and Doherty, P. H.: 2012, Radio Science, 47(1), RS1001, doi:10.1029/2011RS00812.

Bolaji, O. S., Adeniyi, J. O. Adimula, I., Radicella, S. M., and Doherty, P. H.: 2013, J. Atmos. Sol. Terr. Phys., 98, 1, doi:10.1016/j.jastp.2013.02.011.

Bolaji, O. S., Izang, P. A., Oladosu, O. R., Koya, F., Fayose, R. S., and Rabiu, A. B.: 2015, Acta Geophys., 63(3), 884, doi:10.1515/acgeo-2015-0018.

Carter, B. A., Yigenzaw, E., Retterer, J. M., Francis, M., Terkildsen, M., Marshall, R., Norman, R., and Zhang, K.: 2014, J. Geophys. Res., 119(4), 3206, doi:10.1002/2013JA019570.

Chatterjee, S., and Chakraborty, S. K.: 2013, Ann. Geophys., 31, 697, doi:10.5194/angeo-31-697-2013.

Chapman, S., and Bartels, J.: 1940, Geomagnetism (Vol.1 & 2), Oxford University Press.

Chapman, S.: 1951, Arch. Meteorol. Geophys., 4, 368.

De Abreu, A. J., Fagundes, P. R., Gende, M., Bolaji, O. S., De Jesus, R., and Brunini, C.: 2014, Adv. Space Res., 53(9), 1313, doi:10.1016/j.asr.2014.02.011.

Fambitakoye, O., Menvielle, M., and Mazaudier, C.: 1990, J. Geophys. Res., 95, 209.

Fejer, B., and Schierless, L.: 1995, Geophys. Res. Lett., 22(7), 851.

Fejer, B. G., Larsen, M. F., and Farley, D. T.: 1983, Geophys. Res. Lett., 10, 537.

Hofmann-Wellenfof, B., Lichtenegger, H., and Collins, J.: 1992, Global Positioning System: Theory and Practice, Springer-Verlag, Wien, New-York.

Kelley M.C., Ilma, R. R., and Crowley, G.: 2009, Ann. Geophys., 27, 2053.

Jones, K. L.: 1971, J. Atmos. Terr. Phys., 33, 379.

Jones, K. L., and Rishbeth, H.: 1971, J. Atmos. Terr. Phys., 33, 391.

Kikuchi, T., Luehr, H., Kitamura, T., Saka, O., and Schlegel, K.: 1996, J. Geophys. Res., 101, 17161.

Kobéa A. T., Amory-Mazaudier, C., Do, J-M., Lürh, H., Vassal, J., Houngninou, Blanc, E., and Curto, J-J.: 1998, Ann. Geophys., 16, 698.

Kobéa, A. T., Richmond, A. D., Emery, B. A., Peymirat, C., Lürh, H., Moretto, T., Hairston, M., and Amory-Mazaudier, C.: 2000, 1993, J. Geophys. Res., 105(A10), 22979.

Le-Huy, M., and Amory-Mazaudier, C.: 2005, J. Geophys. Res., 10, 10301.

Le Huy, M., and Amory-Mazaudier, C.: 2008, J. of Geophys. Res., 113, A02312, doi:10.1029/2007JA012686.

Mayaud, P.N.: 1980, Derivation, Meaning and Use of Geomagnetic Indices, Geophysical Monograph series, Vol 22, AGU, Washington DC.

Mazaudier C., Blanc, M., Nielsen, E., and Min-Yun, Z.: 1984, J. Geophys. Res., 89, A1, 375.

Mazaudier, C., and Bernard, R.: 1985, J. Geophys. Res., 90, 2885.

Mazaudier, C., Bernard, R., and Venkateswaran, S. V.: 1985, J. Geophys. Res., 90, 6685.

Mazaudier, C., and Venkateswaran, S. V.: 1990, Ann. Geophys., 8, 511.

Mene, N. M., Kobéa, A. T., Obrou, O. K., Zaka, K. Z., Boka, K., Amory-Mazaudier, C., and Assamoi, P.: 2011, Ann. Geophys., 29(12), 2225, doi:10.5194/angeo-29-2225-2011.

Menvielle, M., Iyemori, T., A. Marchaudon, A., and Nosé, M.: 2011, in Geomagnetic Observations and Models, Mandea M. , Korte, Monica (eds.), Geomagnetic indices, Special Sopron Book Series 5, Springer, Dordrecht Heidelberg London New York, doi:10.1007/978-90-481-9858-0_8.

Moeketsi, D. M., Combrinck, W. L., McKinnell, L. A., and Fedrizzi, M.: 2007, Adv. Space Res., 39(5), 821.

Namba, S., and Maeda, K.-I: 1943, Radio Wave Propagation. Corona Publishing, Tokyo, p86.

Nishida, A., Iwasaki, N., and Nagata, N. T.: 1966, Ann. Geophys., 22, 478.

Nishida, A.: 1968, J. Geophys. Res., 73, 1795.

Obrou, O. K., Mene, M .N., and Kobea, A. T.: 2009, Adv. Space Res., 43(11), 1757.

Oladipo, O.A., Adeniyi, A., and Olawepo, J. O., Space weather, 12 (5), 300.

Ouattara, F., Zoundi, C., and Fleury, R.: 2012, Indian Journal Radio & Space Physics, 41, 617.

Peymirat, C., Richmond, A. D., and Kobéa, A. T.: 2000, J. Geophys. Res., 108 (17), 467.

Pi, X., Mannucci, A. J., Lindqwister, U. J., and Ho, C. M.: 1997, Geophys. Res. Lett., 24, 2283.

Richmond , A.D., and Matsushita, S.: 1975, J. Geophys. Res. 80 (19), 2839.

Richmond, A.D., and Roble, R.G. : 1979, J. Atmos. Terr. Phys, 41, 841.

Richmond, A. D., Peymirat, C., and Roble, R. G.: 2003 , 108 (A3), 1118, doi:10.1029/2002JA009758.

Santos, A.M., Abdu, M. A., Sobral, J. H. A., Koga, D., Nogueira, P. A. B., and Candido, C. M. N.: 2012, J. Geophys. Res., 117, A08333, doi: 10.1029/2012JA0117604.

Sastri, J.H.: 1988, Ann. Geophys., 6(6), 635.

Schaer, S.: 1999, Mapping and predicting the Earth's ionosphere using the Global Positioning System, Ph.D. thesis, 228p, Bern University, Bern.

Senior C., and Blanc, M.:1984, J. Geophys. Res., 89, 261.

Shimeis, A., Fathy, I., Amory-Mazaudier, C., Fleury, R., Mahrous, A. M., Yumoto, K., and Groves, K.:2012, J. Geophys. Res., 117, A07309, doi:10.1029/2012JA0117753.

Shimeis, A., Amory-Mazaudier, C., Fleury, R., Mahrous, A. M., and Hassan, A. F.: 2014, Adv. Space Res. 54, 2159.

Shimeis, A., Borries, C., Amory-Mazaudier, C., Fleury, R., Mahrous, A. M., and F. Hassan, F.: 2015, Adv. Space Res. ,55 (9), 2239.
Spiro, R. W., Wolf, R. A., and Fejer, B. G.: 1988, Ann. Geophys., 6, 39.
Stewart, B.: 1882, Terrestrial magnetism, Encyclopedia Britannica (9th ed.), 16, 159.
Su, S-Y, Chao, C. K., and Liu, C. H.: 2007, J. Geophys. Res., 113, A5, doi:10.1029/2007JA012809.
Testud, J. and Vasseur, G.: 1969, Ann. Geophys., 25, 525.
Vasyliunas, V. M.: 1970, in M. McCormac (Ed.), Mathematical models of magnetospheric convection and its coupling to the ionosphere, in Particles and Fields in the Magnetosphere, Springer, New York , p. 60.
Volland, H.: 1979, J. Atmos. Terr. Phys., 41, 853.
Woodman, R. F., and La Hoz, C.: 1976, J. Geophys. Res., 81, 5447.
Woodman, R.: 1970, J. Geophys. Res., 75 (31), 6249.
Yigenzaw, E., Dyson, P. L., Essex, E. A., and Moldwin, M. B.: 2005, Ann. Geophys., 23, 707, doi:1432-0576/ag/2005-23-707.
Zaka, K. Z., Kobéa, A. T., Assamoi, P., Obrou, O. K., Doumbia, V., Boka, K., Adohi, J-P., and Mene, N. M.:2009, Ann. Geophys., 27, 3523.
Zaka, K. Z., Kobéa, A. T., Doumbia, V., Richmond, A. D., Maute, A., Mene, N. M., Obrou, O. K., Adohi, J-P., Assamoi, P., Boka, K., and Amory-Mazaudier, C.:2009, J. Geophys. Res., 115, A11307, doi:10.1629/2010JA015417.
Zaka, K. Z., Kobéa, A. T., Doumbia, V., Richmond, A. D., Maute, A., Mene, N. M., Obrou, O. K., Adohi, J-P., Assamoi, P., Boka, K., and Amory-Mazaudier, C.:2009, J. Geophys. Res., 115, A12314, doi:10.1029/2010JA016292.
Zoundi C., Ouattara, F., Fleury, R., Amory-Mazaudier, C., and Lassudrie-Duchesne, P.: 2012, European Journal of Scientific Research, 77(03), 309.